TU Delft

Delft University of Technology

Experimental analysis of dual-fuel (CH4/H2) capability in a partially-premixed swirl stabilized combustor

Link, Sarah; Dave, Kaushal; Domenico, Francesca de; Rao, Arvind Gangoli; Eitelberg, Georg

DOI
10.1016/j.ijhydene.2024.12.286

Publication date
2025

Document Version
Final published version

Published in
International Journal of Hydrogen Energy

Citation (APA)
Link, S., Dave, K., Domenico, F. D., Rao, A. G., & Eitelberg, G. (2025). Experimental analysis of dual-fuel (CH4/H2) capability in a partially-premixed swirl stabilized combustor. *International Journal of Hydrogen Energy*, *101*, 427-437. https://doi.org/10.1016/j.ijhydene.2024.12.286

Important note
To cite this publication, please use the final published version (if applicable).
Please check the document version above.

Copyright
Other than for strictly personal use, it is not permitted to download, forward or distribute the text or part of it, without the consent of the author(s) and/or copyright holder(s), unless the work is under an open content license such as Creative Commons.

Takedown policy
Please contact us and provide details if you believe this document breaches copyrights.
We will remove access to the work immediately and investigate your claim.

This work is downloaded from Delft University of Technology.
For technical reasons the number of authors shown on this cover page is limited to a maximum of 10.

Green Open Access added to TU Delft Institutional Repository

'You share, we take care!' - Taverne project

https://www.openaccess.nl/en/you-share-we-take-care

Otherwise as indicated in the copyright section: the publisher is the copyright holder of this work and the author uses the Dutch legislation to make this work public.

International Journal of Hydrogen Energy 101 (2025) 427–437

Contents lists available at ScienceDirect

International Journal of Hydrogen Energy

journal homepage: www.elsevier.com/locate/he

Experimental analysis of dual-fuel (CH_4/H_2) capability in a partially-premixed swirl stabilized combustor

Sarah Link *, Kaushal Dave, Francesca de Domenico, Arvind Gangoli Rao, Georg Eitelberg

Flight Performance and Propulsion group, Delft University of Technology, Kluyverweg 1, 2629HS, Delft, The Netherlands

ARTICLE INFO

Keywords:
Dual-fuel combustion
H_2 combustion
Swirl-stabilized combustion
Jet-in cross flow configuration

ABSTRACT

Introducing H_2 as fuel in gas turbines is a promising step towards decarbonizing the energy sector. However, the future availability of H_2 in large quantities remains uncertain. Consequently, designing fuel flexible (CH_4/H_2) combustion chambers for various fuel blends is necessary. The distinct combustion characteristics of H_2, such as high flame speeds and high adiabatic flame temperatures, pose challenges when designing systems that can operate in a stable manner and with low emissions across a wide range of fuel mixtures. This paper investigates the fuel-flexibility of an atmospheric laboratory scale, partially premixed swirl stabilized combustor. By deploying a non-rotating axial air jet (AAI) in the center-line of the swirling flow, the flashback risk for high H_2 content fuels is minimized. This study provides detailed insights into AAI's interaction with CH_4/H_2 fuel blends, analyzing the resulting flow field from Particle Image Velocimetry, emissions from exhaust gas analyser measurements, and flame structures from OH* chemiluminescence and OH Planar Laser Induced Fluorescence. The results show that AAI enables flame stabilization across the full range from 100% CH_4 to 100% H_2 in the same injector geometry. However, a high portion of the total airflow must be injected axially to stabilize H_2 flames. Increasing the level of AAI increases NO emissions and alters flame stabilization mechanisms. This is likely due to a decrease in mixing quality, resulting in the fuel staying close to the periphery of the mixing tube. Switching the fuel from 100% CH_4 to 100% H_2 leads to an increase in NO emission, despite lower adiabatic flame temperatures for the perfectly premixed case. This indicates that the mixing process and flame location within the combustion chamber are essential in controlling NO emissions. Moreover, the flow field transforms significantly from a swirl-stabilized flow field featuring an inner recirculation zone to one resembling the one of a jet flame.

1. Introduction

In the past decade, the interest in hydrogen (H_2) has increased substantially. Largely, due to its carbon-free combustion, it stands out as an attractive choice to conventional fuels in many sectors [1,2]. However, challenges in the production, transportation, and large-scale storage of (green) H_2 [3,4] make the availability of H_2 in the near-term future difficult to predict. Consequently, it is crucial to develop combustion concepts capable of operating with a wide range of fuel mixtures, from entirely conventional fuels to pure H_2. When H_2 is burnt in systems designed for conventional carbon-based fuels, its substantially different combustion properties can have adverse effect on the combustion process and the reliability of the combustor. Higher adiabatic flame temperatures at the same equivalence ratio increase nitric oxide (NO_x) emission. Moreover, the high reactivity and flame speed H_2 can alter the flame position in the combustion chamber. This can potentially affect the mixing of oxidizer and fuel, and in the worst case, lead to flashback [5,6]. Fully premixed combustion systems became the standard in many power generation applications, mainly because they enable low nitric oxide (NO_x) emission. However, especially with fast-burning fuels like H_2, the flashback risk is significantly high to ensure safe operation [7]. Partially premixed combustion, achieved by injecting the fuel as late as possible upstream of the combustion chamber, is a widely used approach to keep NO_x emissions low while minimizing the flashback risk. Nonetheless, achieving rapid mixing of fuel and oxidizer before entering the combustion chamber remains a significant challenge. Innovative injector designs, like micro-mix, have been proposed [8], where the fuel gets injected in jet-in cross-flow (JICF) configuration into the air through small air guiding panel structures. The fuel injection through multiple miniaturized fuel jets results in the formation of micro flames, producing low NO_x emissions and providing inherent safety against flashback. Nevertheless, this solution requires significant modifications to the combustion chamber geometry

* Corresponding author.
E-mail address: s.j.link@tudelft.nl (S. Link).

https://doi.org/10.1016/j.ijhydene.2024.12.286
Received 27 September 2024; Received in revised form 15 November 2024; Accepted 16 December 2024
Available online 1 January 2025
0360-3199/© 2024 Published by Elsevier Ltd on behalf of Hydrogen Energy Publications LLC.

and introduces a high pressure drop across the injector, which negatively impacts gas turbine performance. As a stopgap solution existing injector geometries can be modified, to be able to accommodate a range of mixtures of conventional fuel and H_2. Swirl stabilized combustion is the most suitable form of flame stabilization in modern gas turbines, by aerodynamically stabilizing the flame in the combustion chamber away from solid components [9]. The swirl number Sw is defined as the ratio of the axial flux of tangential momentum to the axial flux of axial momentum. Strongly swirling flows are characterized by substantial radial and axial pressure gradients: above a critical swirl number, these result in the formation of an inner recirculation zone (IRZ) [10]. Due to low velocities in the IRZ and the transport of radicals back to the reaction zone, flames can be aerodynamically stabilized even in lean conditions.

However, the low-velocity region in the core of the swirling flows increases the propensity to flashback, particularly for highly reactive fuels like H_2. High swirl numbers are especially prone to flashback, due to a strong velocity deficit on the centerline of the swirling flow and the increased risk of flashback due to combustion-induced vortex breakdown [11]. Several strategies were proposed to decrease the flashback propensity, such as axial injection of a central air jet (AAI). This axial jet decreases the flashback propensity by decreasing the velocity deficit on the center line of the swirling flow and by shifting stagnation point of the IRZ downstream, preventing flashback due to combustion-induced vortex breakdown [12]. Reichel et al. [13,14] experimentally demonstrated that AAI improves the flashback resistance for H_2 flames while keeping the NO_x emissions below 10 ppm in the exhaust. Another option to overcome the velocity deficit on the center line is injecting a part of the fuel in axial direction on the centerline, as implemented by the Siemens SGT-700/800 burner [15]. However, this might lead to a fuel-rich core, which can result in a steep rise in emissions. More recently, the HYLON injection system has shown promising results in stabilizing a 100% H_2 flame for selected operating conditions, by injecting H_2 non-premixed swirled through a central pipe a few millimeters before the combustion chamber [16,17]. However, the scalability to higher power settings or a higher technology readiness level (TRL) remains uncertain due to the multitude of design variables in the set-up.

Several studies investigated the effect of H_2 enrichment on CH_4 flames in swirl stabilized burners. Under perfectly premixed conditions it has been observed that H_2 addition lowers the equivalence ratio for both lean blow-off and flashback limits, primarily due to increased reaction rates and flame speeds [18–20]. This is also the reason why the flames become shorter and more compact flames with increasing level of H_2 [19,21]. Liu et al. [22] showed that H_2 addition triggers a flame shape transition from M-flame to Π-flame. This changes the flashback mode from flashback due to combustion induced vortex breakdown to boundary layer flashback. Similarly, An et al. [23] investigated the effect of H_2 enrichment on the flame shapes in a laboratory-scale low-swirl burner. Mao et al. [24] observed that for increasing H_2-content, the flame moves upstream in the outer shear layer (OSL) and finally anchors as an M-flame on the injector rim. In the study of Guo et al. [25] it has been shown that H_2 addition increases the OH-radical concentration and the overall reaction rate in the reaction zone. This is expected to reduce the strength of the inner recirculation zone (IRZ) [26,27] due to a high acceleration of the flow, leading to increased temperatures in the reaction zone. Consequently, this leads to rising NO_x emission values for increasing H_2 contents, despite decreasing adiabatic flame temperatures and decreasing residence times in the reaction zone. It also has been shown numerically that H_2 addition can largely increase the NO formation via the NHH pathway [28], which can contribute significantly to the overall NO emissions [29].

However, most studies on H_2 enriched CH_4/air-swirling flames have not investigated H_2 contents exceeding 80% by volume [30]. Given the low molecular weight of H_2, transitioning from 80% to 100% H_2 represents a significant change in fuel composition (in mass and energy content). This alteration affects both the chemical and the physical processes occurring in the reacting flow, thereby posing considerable challenges for combustor operations.

Currently, there is limited experimental work available, which comprehensively studies lean partially premixed combustion across the entire range from 100% CH_4 to 100% H_2. Therefore, addressing the challenges associated with burning a wide range of H_2-enriched fuel content fuels in a conventional swirl stabilized geometries remains largely open. The presented burner operates at atmospheric conditions and employs fuel injection in jet-in cross-flow configuration (JICF) configuration. JICF, where fuel is injected perpendicular to the airflow, has emerged as one of the most promising solutions to mix two fluids in a limited space [31]. This work is novel in its exploration of dual-fuel combustion with JICF injection combined with axial air injection (AAI). The distinct combustion properties of CH_4 and H_2 are expected to significantly impact the flame properties, and consequently the interaction with AAI. Furthermore, the mixing performance of the JICF is anticipated to be strongly influenced by the fuel jet properties, which can, in turn, affect the overall combustor performance. This study aims to provide insights into the performance of the AAI concept across a wide range of fuel compositions, by examining the flow field, the flame shapes, and the NO emissions.

Various measurement techniques, including OH-Planar laser-induced fluorescence (OH-PLIF), particle image velocimetry (PIV), OH* Chemiluminescence, and an exhaust gas emission analysis are employed to provide valuable insights into flame/flow interactions for different fuel mixtures and into the effect of AAI on the burner performance. To further comprehend the influence of the swirl number in combination with AAI, experiments are conducted with two different swirl numbers.

The paper is structured as follows: Section 2 presents an overview of the experimental setup and the measurement techniques. Section 3 discusses the effect of H_2 enrichment and AAI on the operational range, flame/flow interactions, and emissions. Finally, Section 4 summarizes the most important findings of this study.

2. Experimental set-up

In this section, the experimental set-up, as well as the diagnostics techniques used to characterize the burner, are described.

2.1. Burner geometry and operating conditions

Reacting experiments were conducted in an atmospheric laboratory scale combustor with a partially premixed single-stage axial swirler at the sustainable aircraft propulsion laboratory of TU Delft [32,33]. A schematic of the set-up is provided in Fig. 1. The outlet of the combustor connects to a flexible exhaust with an inner diameter of 150 mm and a length of 1.6 m. The combustor is operated in a partially premixed configuration. The combustion air gets supplied upstream of the fuel injection through an axial swirler with an axial air jet on the centerline of the swirling flow [13]. The axial air jet (AAI) is injected through an 8 mm diameter port on the centerline of the swirling flow. The axial airflow is a part of the total air available for combustion and is therefore always given as the percentage of the total air mass flow rate $\chi = \dot{m}_{AAI}/(\dot{m}_{swirl} + \dot{m}_{AAI})$.

The axial swirler, which surrounds the axial air port is designed with swirl numbers of 0.7 and 1.1 based on [34]

$$Sw = \frac{G_\theta}{R_n \cdot G_x} = 0.5 \frac{1}{1-\psi} \frac{1-(R_h/R_n)^4}{(R_h/R_n)^2} tan(\phi_0) \quad (1)$$

with G_Θ being the axial flux of tangential momentum, G_x the axial thrust, ψ the blockage factor, Φ_0 the tip vane angle and R_n and R_h respectively the outer and hub radius of the swirler vanes ($R_n = 12$ mm

Table 1
Operating conditions for the design points at constant air flow rate.

Design points at P = 12 kW and $\dot{m}_{air}$ = 5.1 ·10^{-3} kg/s						
Tag	XH_2	U_∞ [m/s]	ϕ	T_{ad} [K]	J	ρ_{react}/ρ_{prod}
A	0	10.45	0.75	1942	0.48	6.40
B	0.25	10.62	0.74	1930	0.55	6.33
C	0.4	10.75	0.73	1921	0.61	6.26
D	0.6	11.01	0.71	1908	0.68	6.13
E	0.8	11.44	0.68	1895	0.75	5.94
F	1	12.26	0.62	1858	0.67	5.60

and R_h = 5 mm). G_x and G_θ can be obtained by solving the following equations

$$G_x = 2\pi \int_0^R \rho U^2 r dr$$
$$G_\theta = 2\pi \int_0^R \rho U V r^2 dr \quad (2)$$

The burner operates on different fuel mixtures (CH_4 and H_2) injected through four nozzles with a diameter of d_{fuel} = 3.175 mm in jet-in cross-flow configuration into the swirling flow, 6 mm downstream of the swirler exit. The mixing process of fuel and oxidizer takes place in the mixing tube with a diameter d_{MT} = 24 mm and length l_{MT} = 60 mm. Due to a low momentum flux ratio $J = \rho_{fuel} \cdot u_{fuel}^2 / \rho_{air} \cdot u_{air}^2$ [35] and a short mixing tube, the mixture is anticipated to be partially premixed when entering the combustion chamber. Furthermore, it is expected that the mixing process is influenced by the density ratio between the jet and swirling flow [35] as well as the level of axial air injection [13].

Downstream of the mixing tube, the fuel–air mixture then enters the optically accessible quartz combustion chamber (d_{CC} = 150 mm and l_{CC} = 400 mm). At the reference case the combustor operates with CH_4 at an equivalence ratio ϕ = 0.75 at a power of P = 12 kW (corresponding to a total air flow of $\dot{m}_{air}$ = 5.1 ·10^{-3} kg/s and fuel flow $\dot{m}_{CH4}$ = 2.2 ·10^{-4} kg/s). The mass flow rates for both fuel and air are controlled by Bronkhorst digital mass flow meters with an accuracy of ±0.5% RD plus ±0.1% FS. Due to the flow rate limitations of the CH_4 mass flow controller, it was not possible to reach operating conditions between 85% and 100% H_2.

When H_2 is added to CH_4, the thermal power P and the total air mass flow rate $\dot{m}_{air}$ are kept constant. The overall equivalence ratio for the mixture is calculated with

$$\phi = s \frac{\dot{m}_{CH_4} + \dot{m}_{H_2}}{\dot{m}_{air}} \quad (3)$$

The stoichiometric ratio s is defined as:

$$s = \frac{(2 - 1.5X_{H_2})(W_{O2} + 3.76W_{N2})}{X_{CH_4}W_{CH_4} + X_{H_2}W_{H_2}} \quad (4)$$

with X_{H_2} and X_{CH_4} being the mole fractions of H_2 and CH_4 in the fuel mixture, and W the molar masses. The Reynolds number with respect to the mixing tube diameter is around Re = 16,000 for the conditions at P = 12 kW.

Table 1 shows an overview of the operating conditions at the design point of 12 kW for different H_2 contents XH_2, including the equivalence ratio ϕ, the adiabatic flame temperature T_{ad}, the momentum flux ratio J and the thermal expansion ratio. T_{ad} and the thermal expansion ratio ρ_{react}/ρ_{prod} were calculated for laminar premixed flames with CANTERA [36] using GRI 3.0. Table 1 shows, that ϕ, T_{ad} and the thermal expansion ratio are decreasing for increasing XH_2. Due to the increased volumetric flow rate of the fuel for increasing XH_2, the bulk velocity in the mixing tube is increased. The highest value for J is for XH_2 = 0.8. The points were tested at three different levels of AAI, 0%, 10%, and 20% for the two different swirl numbers. If no flashback occurred, measurements have been taken for the corresponding operating conditions.

2.2. Measurement techniques

Particle imaging velocimetry (PIV)

Flow fields in the center plane under reacting conditions were obtained using 2D2C Particle Image velocimetry (PIV). TiO_2 particles with a size of 0.5-1 μm were introduced into the swirling air stream as seeding particles. The particles were illuminated by a 527 nm high-repetition-rate (850 Hz) laser with a pulse energy of 30 mJ and a pulse width of <200 ns (Quantronix Darwin Duo 527-80-M). The thickness of the laser sheet was around 2 mm to minimize out-of-plane particle displacement between the two laser pulses. The two pulses had a Δt of 37 μs. The scattered light was captured by a LaVision Imager pro HS4M camera (sensor size 2016 *x* 2016 pixels) with a repetition rate of 850 Hz. This results in a resolution of 24.35 pix/mm. The camera was mounted with a macro lens (180 mm, fstop 2.8) and equipped with a bandpass filter 532 ±10 nm. The raw images were scaled using a calibration image and then background-corrected by applying a minimum sliding background subtraction over nine images. The velocity fields were computed with the cross-correlation algorithm (LaVision, Davis 10 software). A multipass cross-correlation approach with decreasing interrogation window size (from 96 *x* 96 to 32 *x* 32 pixels) is applied to obtain the instantaneous velocity vectors. The final interrogation window size with 50% overlap yields a vector spacing of approximately 0.83 mm. The data was filtered for outliers (Davis 10 universal outlier detection with median filter) and interpolated from adjacent interrogation areas. The velocity fields are averaged over 2000 images and normalized by the bulk velocity in the mixing tube U_{MT}.

The systematic error of PIV was examined by correlation statistics method (LaVision, Davis 10 software) and the results indicate that the estimated uncertainties of velocities are lower than 5.0%.

OH chemiluminescence*

The OH* signal was captured with a Tucsen CMOS camera, equipped with a UV lens and an optical filter with a width of 50 nm, centered at 325 nm. The images were acquired at a frequency of 10 Hz. The inverse Abel transform [37] was applied to time-averaged OH* results (over 100 single shot images) so that the distribution of OH* signal on the symmetric plane of the flame was obtained. This OH* distribution can be used as an indicator of the location of heat release [38]. For the Abel transform, each image is first normalized by the maximum pixel value of the image. After the Abel transform, the signal is again normalized by its maximum value, and a smoothing filter with a filter size of 25x25 pixels is applied. This reduces the noise caused by the Abel transform but did not distort the shape of the flame.

OH-PLIF

The OH-PLIF measurements were performed by exciting the Q1(8) transition of the OH radicals with 283.55 nm laser radiation. A frequency-doubled (532 nm) Nd:YAG laser (Q-Smart 850 from Quantel) was used to pump a tunable dye laser (Sirah Cobra Stretch), operated with Rhodamine 590 dye. The dye laser output (566 nm) was then frequency-doubled and tuned to the Q1 (8) transition. A laser sheet, approximately 100 mm high and 1.5 mm thick, was formed using sheet forming optics. A CMOS camera (LaVision Imager M-lite 5M) detected the OH-PLIF signal. The signal was intensified with a LaVision IRO X module (gate time 100 ns, Gain 60%), equipped with a UV camera lens (f/2.8, focal length 85 mm). A narrowband filter with 80% transmission was placed in front of the intensifier, to capture the signal at 308 nm. For each operating condition, 500 single-shot PLIF images were collected at a frequency of 10 Hz. The images were corrected for variations in laser sheet intensity using the flat field function in Davis. The laser sheet within the combustion chamber was mapped by filling the chamber with acetone vapor. The scaling factor of the acquired images results in 0.11 mm/pixel.

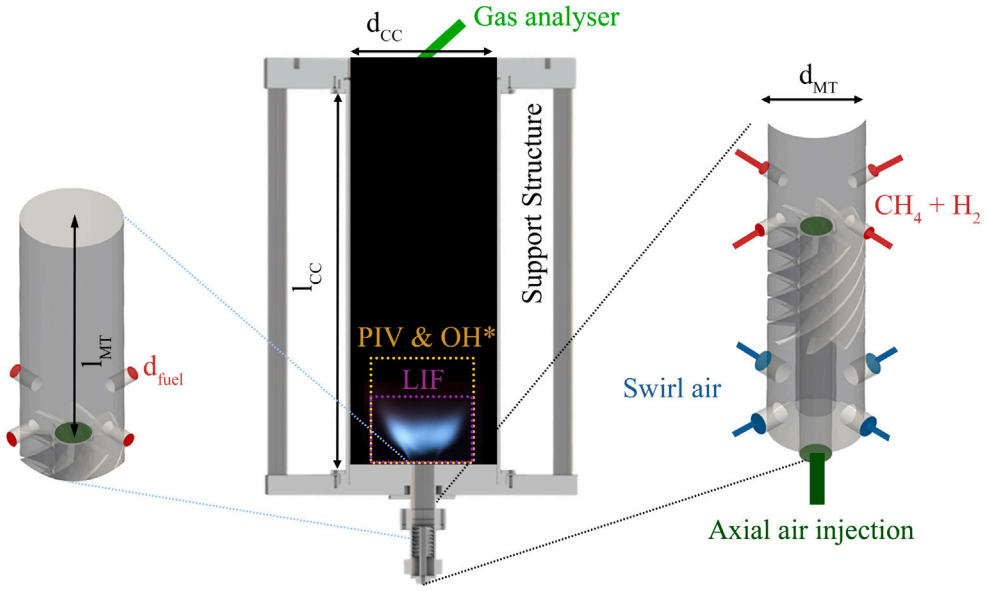

Fig. 1. Schematic TU Delft swirl burner with a detailed view of the injector and the location of the measurement techniques.

Gas analyser

Emission measurements were acquired with an ABB AO2000 gas analyser, equipped with the modules Limas21 HW (NO and NO_2 - accuracy 0.1 ppm), Uras26 (CH_4 - accuracy 0.1 vol%, CO - accuracy 1 ppm, CO_2 - accuracy 0.1 vol%), and Magnos28 (O_2- accuracy 0.1 vol%). The exhaust gas was sampled in the center of the outlet plane of the combustion chamber. A recalibration of the gas analyser with designated calibration gases was performed before each measurement day, in order to reduce uncertainties due to zero drift and sensitivity drift. For all three modules, the linear deviation is $\leq 2\%$ of the span and the repeatability $\leq 1\%$. The emission values were averaged over a time span of at least 30 s, once stationary conditions for the set point were reached. The averaged values were normalized by a volumetric fraction of 15% O_2 in the flue gases. CO and CH_4 values were measured below 4 ppm and 15 ppm, respectively, which are the detection limits of the gas analyser. Due to their low values, these emission values are not discussed and it is assumed that complete combustion took place. NO_2 for all points was below 2 ppm. In some cases, the values of NO_2 are not representative, because the dew temperature increased with increasing concentrations of water vapor in the products. For high H_2-content fuels, this temperature exceeded the product temperature in the gas analyser (80 °C). This most likely led the water to condensate, creating significant uncertainties due to NO_2 dissolving in water. Additionally, NO_2 is well known to react with liquid water to form nitric acid and nitrous acid [39]. NO on the other hand remains largely inert and has a limited solubility in water. Given that, for 100% CH_4 the NO_2 value is an order of magnitude lower than NO, it is assumed that NO is the primary contributor to NO_x emissions. Consequently, it was decided to compare combustion performance by focusing on NO emissions.

3. Results

The results chapter first explores the operational range of the proposed lean partially premixed set-up, focusing on the flashback and blowout limits across various equivalence ratios ϕ and H_2 contents at different levels of AAI. Following this, flow fields obtained by PIV are discussed, highlighting the effects of H_2 enrichment on the average flow fields within the combustion chamber. Next, OH* chemiluminescence and PLIF images illustrate the different flame stabilization mechanisms and the location of the flame in the flow field. Finally, the combustor performance is evaluated under different operating conditions by analyzing the measured NO emissions.

3.1. Operational range

In this section, the operational range of the combustor is discussed. Only lean conditions have been tested, as this is the intended operational regime for this set-up. Additionally, the low bulk velocities in the mixing tube (approximately 10 m/s) would not allow the operation of the setup with high H_2 content fuels near stoichiometric conditions. Fig. 2 presents the stability map of Sw = 1.1 at a constant air flow rate of $\dot{m}_{air} = 5.1 \cdot 10^{-3}$ kg/s, examining the cases with $\chi = 0\%$ and $\chi = 20\%$. The stability map indicates the stable region, the lean blowoff limits (LBO), and the flashback limits (FB). The stability analysis in this paper focuses on static stability, thus excluding consideration of thermoacoustic instabilities in the analysis. Therefore, even if a flame is classified as statically stable, it could still manifest thermoacoustic instabilities. Static stable flames stabilize downstream of the mixing tube exit. Flashback is typically defined as the uncontrolled upstream propagation of the flamefront, caused by an imbalance of local burning velocity and local flow speed [40]. In the current set-up, the short distance from the fuel injection location to the combustion chamber prevents flames from traveling far upstream. Therefore, in this study, flames exhibiting flashback are identified by the presence of an upstream flame front within the mixing tube. The flame burning in the mixing tube is undesired, as it can impose high thermal loads on the combustor components, potentially leading to material failure.

The images above the stability map display the average natural emissions of the flame, captured with a Nikon 7500 DSLR camera fitted with an AF-S DX NIKKOR 18-140 mm telephoto lens. Each image represents an average of 30 snapshots. An example of a stable flame at $\chi = 0\%$ is marked with a ⋆. An example of a flame in flashback mode can be seen marked with the red triangle Δ for the $\chi = 0\%$ case.

For $\chi = 0\%$, only a narrow operational range of stable combustion can be identified. It is observed that increasing the H_2 content reduces the critical ϕ for the lean blowout limit. This decrease results from the increase in reaction rate, the increase in diffusivity and burning velocity for H_2-enriched flames. This can be seen as an advantage, as a lower lean blowout allows the combustor to be operated at leaner conditions, thus lowering the formation of thermal NO_x. However, due to a higher flame speed, it also decreases the equivalence ratio for the flashback limits, as shown in Fig. 2. Flames above $XH_2 = 0.8$ cannot be stabilized without AAI, even at very lean conditions($\phi = 0.38$). When the overall equivalence ratio is increased to $\phi = 0.65$, flames can only be stabilized up to $XH_2 = 0.4$.

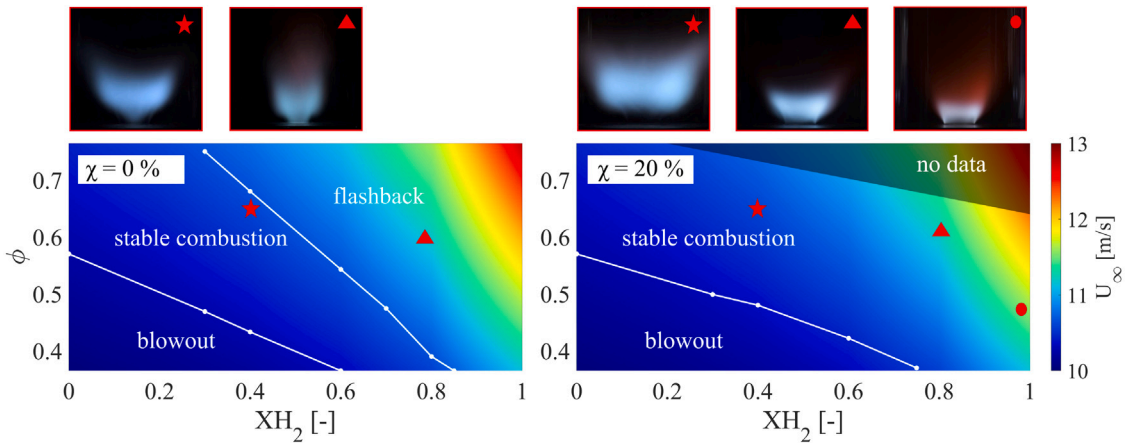

Fig. 2. Stability map for Sw = 1.1 at a constant air mass flow rate with average images of natural emissions of example static stable and unstable flames.

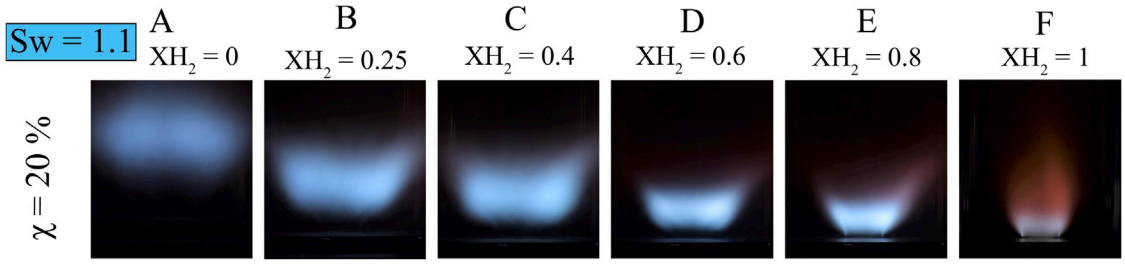

Fig. 3. Effect of H_2 enrichment on the flame shape for at P = 12 kW, Sw = 1.1, AAI = 20%. Natural emission in the visible spectrum.

The introduction of AAI, instead, allows full operational range from 100% CH_4 to 100% H_2 (Fig. 2). When a high level of AAI is introduced (χ = 20%), flashback does not occur within the investigated range of XH_2 and ϕ. For the case with XH_2 = 0.4 (⋆), the flame is significantly lifted off the injector. With at least χ = 20%, flames can even be stabilized reliably up to XH_2 = 1 across the entire range of investigated ϕ. Lower levels of AAI have resulted in flashback when ϕ reached a critical value.

Fig. 3 illustrates the average images of the natural emissions of the flame at χ = 20% with varying H_2 content. As the H_2 content in the fuel increases, the flame becomes compact and is located closer to the injector, due to the higher flame speed and reactivity of H_2-rich fuels. Noticeably the reddish color resulting from H_2O* Chemiluminescence [41] is more intense with increased H_2 content, due to the greater amount of water vapor in the products. The color of the reaction zone transitions from blue, for fuels with high CH_4 content (CH* Chemiluminescence) to gray for 100% H_2 (presumably a result of H_2O_2* Chemiluminescence [42]).

For the lower geometric swirl number of Sw = 0.7, less AAI is required to stabilize the flame at high H_2 contents. This is expected, as the swirl induces a radial pressure gradient that balances the centrifugal force. As a consequence, a higher swirl number also introduces a higher adverse axial pressure gradient, resulting in an upstream location of the stagnation point. This can be seen in Fig. 4, which shows the flame shapes for Sw = 0.7 and Sw = 1.1 for χ = 10% at different XH_2. The medium level of AAI (χ = 10%) was chosen for comparison, because for Sw = 0.7, χ = 20% the flame is lifted far off the injector, causing the flame to become unstable. Such high levels of AAI are expected to suppress the IRZ, by reducing the swirl number below the critical value for vortex breakdown of Sw = 0.6 [43].

For the same level of AAI, the lift-off height is increased for the lower swirl number. For the lower swirl number, the burner can be operated across the entire range of H_2-contents, while for the higher swirl number, the flame is experiencing flashback above XH_2 = 0.6. Notably, at the lower swirl number, the flame is attached to the outer radius of the mixing tube, suggesting stabilization of the flame in the boundary layer of the mixing tube. Conversely, at the higher swirl number, the flame stabilizes more towards the center of the swirling flow.

3.1.1. Flow field analysis

In Fig. 5 the average streamwise velocity plots are shown for Sw = 1.1 at various H_2 contents at the design conditions presented in Table 1. Sw = 0.7 has a similar behavior at lower levels of AAI (not shown here). The scale of the colored background indicates the normalized streamwise velocity, which is superimposed with the streamlines calculated from the x- and y-component of the velocity. In a swirl-stabilized burner with a high swirl number (Sw > 0.6), the flow field is usually characterized by an inner recirculation zone (IRZ), which forms as a consequence of vortex breakdown. The IRZ serves as an aerodynamic flame holder, allowing flames to stabilize away from the solid components of the combustor.

The figure illustrates a notable alteration in flow field shape with increasing H_2 content. The case with XH_2 = 0 (Case A) exhibits a flow field featuring an IRZ, which can be seen as the area of negative axial velocities in Fig. 5. This feature fully disappears for the case with XH_2 = 1 (Case F). For the cases with CH_4/H_2 mixtures, the strength of the IRZ diminishes with increasing H_2 content. The drastic change in flow field structure from case E to case F is a consequence of expressing the fuel composition in volume fraction. Case E (XH_2 = 0.8) corresponds to a mass fraction of YH_2 = 0.33, leaving a big gap between case E and the pure H_2 case (Case F).

Additionally, the flow fields illustrate that increasing H_2 content in the fuel increases the maximum axial velocity magnitude. In case A, the maximum axial velocity is around 1.3 U_{MT-CH4}, while it exceeds 2 U_{MT-H2} for case F. This indicates a stronger thermal expansion due to heat release for case F, which correlates with the decrease in size and strength of the IRZ as the H_2 content increases.

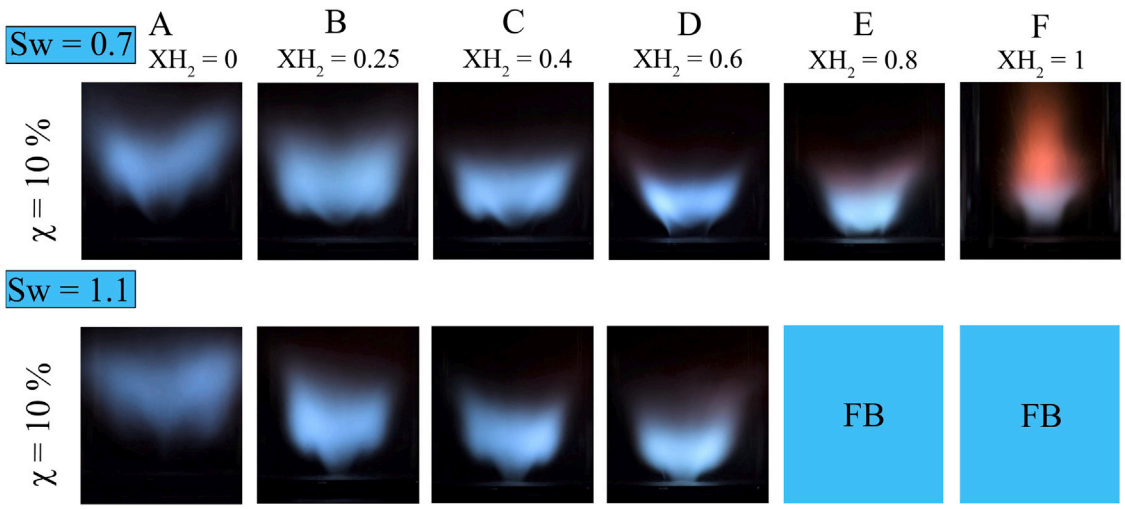

Fig. 4. Effect of the swirl number on the flame shape for at P = 12 kW, XH_2. Average image of natural emission in the visible spectrum. FB = flames exhibiting flashback.

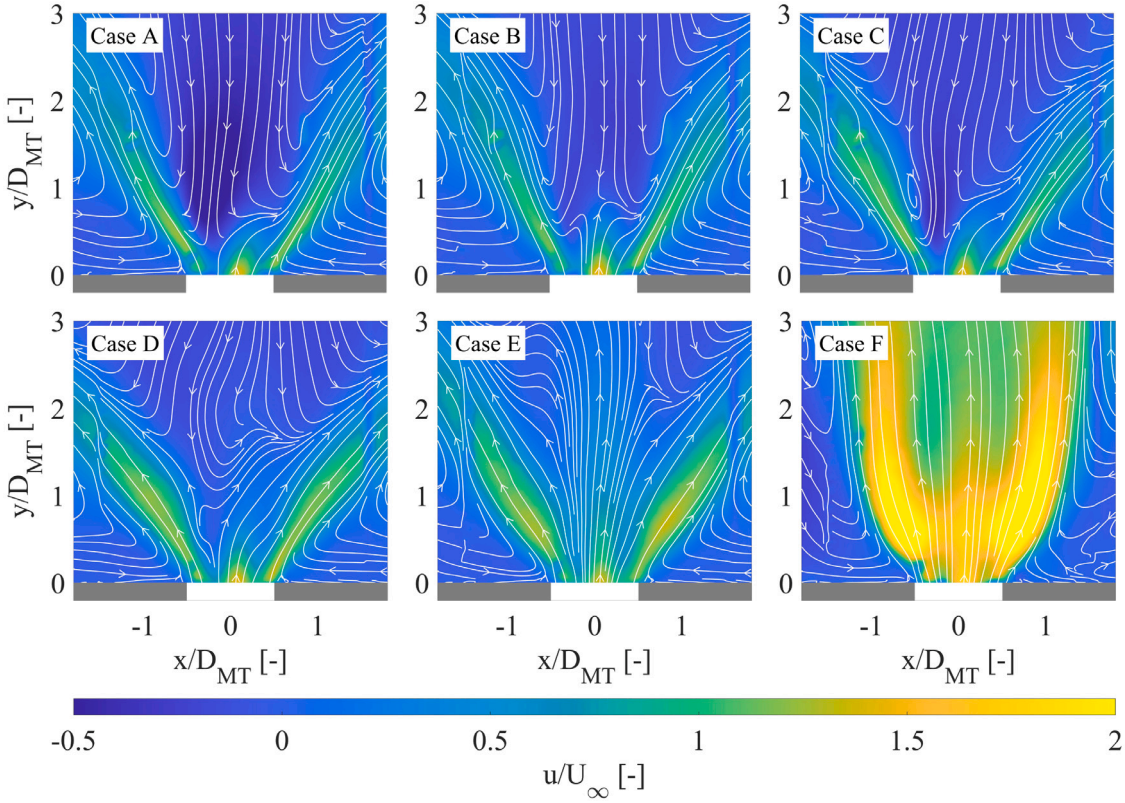

Fig. 5. Average streamwise velocity fields in reacting conditions superimposed with streamlines, obtained from PIV at with Sw = 1.1, P = 12 kW for different XH_2 at χ = 20%.

Increasing the H_2 content can be seen to induce a strong axial feature to the flow emerging from the mixing tube, as seen in Fig. 5 from the streamlines ($-0.5 \leq x/D \leq 0.5$). Specifically, cases E and F show a strong axial jet-like structure at the mixing tube outlet that suppresses the IRZ seen prominently in the other cases.

When changing the fuel from CH_4 to H_2, multiple aspects influence the flow field. Firstly, the momentum flux ratio J between the fuel and the swirling flow changes. Due to the radial fuel injection, it is expected that an increase in momentum flux ratio (J) decreases the effective swirl number. Additionally, the thermal expansion ratio has been shown to decrease the swirl number, due to a greater acceleration of the flow in the axial direction [44]. A similar behavior also has been observed in the work of Shoji et al. [45], where increasing the equivalence ratio ϕ of a low-swirl H_2 flame resulted in the formation of widespread high-velocity regions. This is attributed to an increased thermal expansion ratio due to an increase in ϕ and due to a reduced lift-off height of the flame, which causes an intense thermal expansion of the gas very close to the injector. Table 1 summarizes the ratios for J and the thermal expansion ratios calculated for perfectly premixed conditions for the operating conditions at P = 12 kW. As described previously, J has its maximum value at $XH_2 = 0.8$. The thermal expansion ratio decreases for increasing H_2 content. However, it is expected that due to the short mixing tube and the low J [35], the location of the flame front determines significantly the equivalence ratio at which the reaction takes place. A flame front positioned upstream, or even an attached flame front to the rim (as it is for case F), is expected to burn

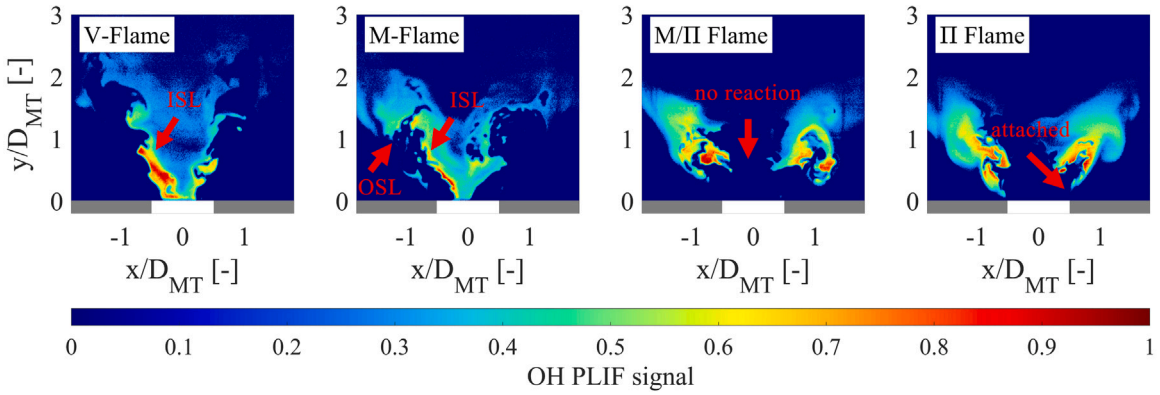

Fig. 6. Instantaneous OH-PLIF images of flame types observed in this study with Sw = 1.1 at P = 12 kW, **V-Flame**: XH_2 = 0, χ = 0% | **M-Flame**: XH_2 = 0.4, χ = 10% | **M/Π-Flame**: XH_2 = 0.4, χ = 20% | **Π-Flame**: XH_2 = 0.8, χ = 20%.

in a much richer condition than the nominal equivalence ratio. For a lifted flame, like case A, there is more time for fuel and oxidizer to mix, consequently, the flame will burn at an equivalence ratio closer to the nominal one. Additionally, the location in the flow field determines the magnitude of the local flow speed at the flame front. A flame located close to the mixing tube outlet will consequently accelerate the flow to higher axial velocities downstream of the flame compared to a lifted flame. The flow field for case F resembles that of the low-swirl flame discussed in [45]. This similarity suggests that the increased thermal expansion in case F reduces the swirl number to a level typical of a low-swirl flame, resulting in the absence of an IRZ.

3.2. Flame stabilization

Flame types

Fig. 6 shows the instantaneous OH-PLIF images of the different flame shapes observed in the experiment. The flame shapes are identified through single-shot OH-PLIF images, providing clear insights into the mechanisms responsible for flame stabilization. OH* Chemiluminescence images offer a less detailed, line-of-sight averaged perspective, making it more difficult to distinguish specific flame features. The V-flame shape (XH_2 = 0, χ = 0%) is similar to the ones in literature. For a V-flame shape, the flame is stabilized in the inner shear layer (ISL) and the flame trailing edge tip is pointing towards the exit of the combustion chamber [46]. Additionally, the flame is attached to the rim in the ISL. For an M-flame (XH_2 = 0.4, χ = 10%), the flame trailing-edge tip protrudes in the outer shear layer (OSL), pointing towards the combustion chamber dump plane. When the fuel contains a high amount of H_2 or when the mixing is reduced due to an increased accumulation of fuel close to the periphery of the mixing tube, the flame can stabilize in the OSL, due to lower chemical time scales τ_{chem}. The flames in the OSL are strongly affected by heat losses, which quenches the reactions for low H_2 contents or lean conditions. In contrast to the definition in literature, the flame in the outer shear layer is not attached to the injector, presumably due to heat losses to the steel baseplate [47]. Nevertheless, the flame will be classified as M-flame, as it is attached to the injector in the ISL, and is clearly protruding into the outer shear layer. For a Π-Flame (XH_2 = 0.8, χ = 20%), the flame front on the center is pushed downstream, while the flame is attached to the outer rim. This type of flame has been observed and described in Liu et al. [22]. In comparison to their work, however, for the Π-flame presented here no reaction takes place on the center-line of the swirling flow. Both, high axial velocities due to AAI and lean quenching due to imperfect mixing on the centerline partly contribute to this effect. This will be discussed later in this section. Since the flame is attached to the outer rim of the injector, the risk of boundary layer flashback is significantly higher compared to an M-flame. A flame, where the flame front on the centerline is pushed downstream, but the flame is not attached to the outer radius will be called M/Π Flame (XH_2 = 0.4, χ = 20%).

Effect of axial air injection

The flame structure is initially investigated for a fixed H_2 content to analyze the effect of AAI. Images were taken in the emissions band λ = 320 nm ± 25 nm, centered at the OH* Chemiluminescence signal to study the reaction zone. The Abel deconvoluted images can be considered as a good indication of the location of a heat release zone in the axial plane of the burner, and are therefore used to determine the location of the flame in the flow field [38].

Fig. 7 shows the Abel deconvoluted OH* images with superimposed streamlines obtained from PIV measurements for different levels of AAI at XH_2 = 0.4. The flame in Fig. 7 represents a V-flame shape for χ = 0%. Throughout the investigated range, for χ = 0%, only V-flames occurred. The stagnation point being inside the mixing tube and the low velocities on the centerline of the swirling flow allowed the flame burn attached to the injector, even in the case with no H_2. For the intermediate level of AAI (χ = 10%), the flame burns in the ISL but develops small branches in the OSL. The flame classification presented in the previous section shows that this is an M-flame. This outcome is anticipated due to reduced mixing, causing increased accumulation of fuel close to the periphery of the mixing tube, thereby facilitating stabilization of the flame in the OSL. For χ =20%, the flame is lifted off the injector and partially burns in the inner shear and outer shear layer (OSL), transitioning to an M/Π-flame.

As it has been thoroughly discussed in [13], increasing the level of AAI shifts the location of vortex breakdown further downstream and reduces the negative axial velocity on the centerline. For χ = 20% in Fig. 7, the flow field even exhibits a region of positive axial velocity around the injector outlet section between $-0.5 \leq x/D \leq 0.5$. The significant change in the flow field between χ = 10% to χ = 20% can be explained by the non-linear effect of AAI on the swirl number. For lower levels of AAI, the effect on the swirl number for increasing AAI is smaller than for high levels of AAI, as confirmed in [48]. Additionally, it can be seen that the flame up to χ = 10% is burning on the centerline, while for χ = 20% no reaction takes place on the centerline, despite low velocities being present. It is anticipated, that the introduction of a high-momentum jet (compared to the momentum of the fuel) on the centerline will result in a decrease of the mixing quality [14]. This indicates that the flame is extinguished on the centerline, as a consequence of a decrease in mixing quality with an increasing level of AAI. Additionally, flames with an increasing level of AAI burn more in the OSL, supporting the assumption of a fuel-richer area close to the periphery of the mixing tube, as AAI levels increase.

Effect of H_2-content

Fig. 8 shows the Abel deconvoluted images for different H_2 contents. Due to the high level of AAI (χ = 20%) the flames are lifted off the injector for almost all the cases, except for 100% H_2 (Case F). When

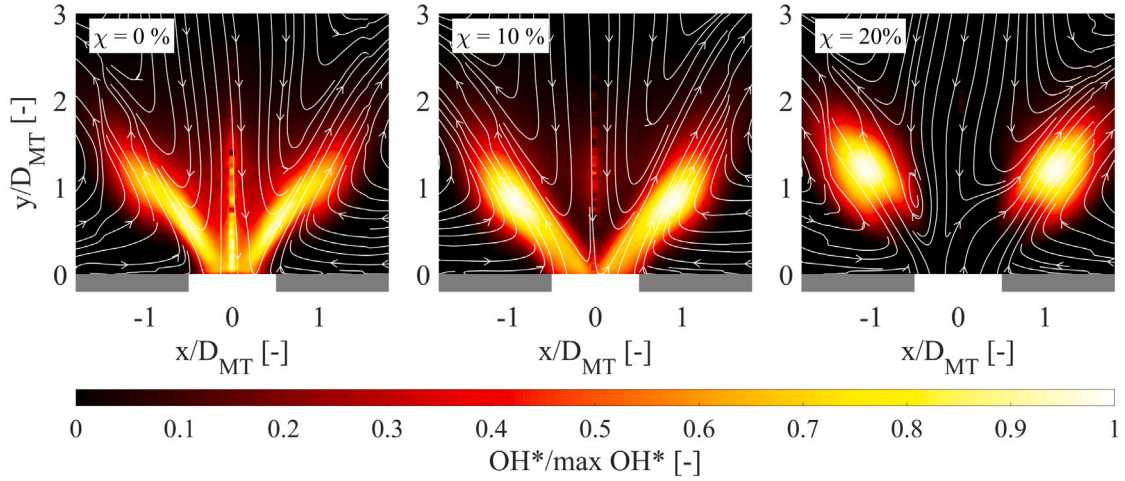

Fig. 7. Abel deconvoluted OH* images for Sw = 1.1 at for case C at P = 12 kW for XH_2 = 0.4 with different levels of χ, superimposed with streamlines.

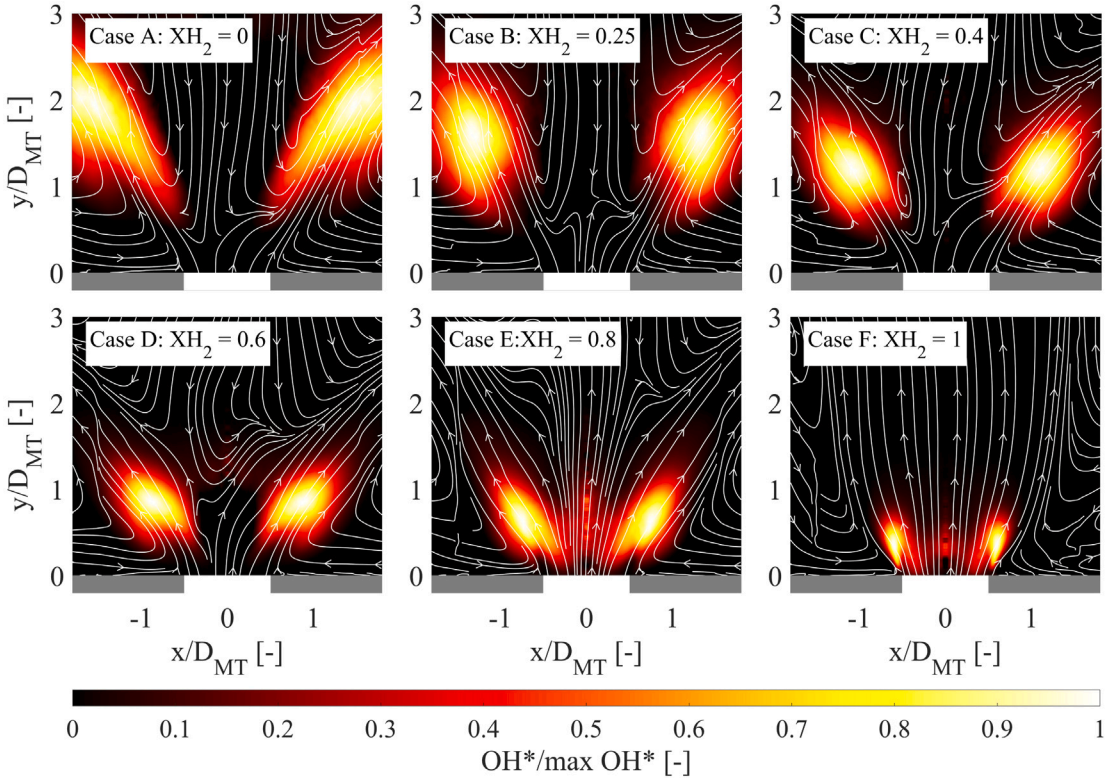

Fig. 8. Abel deconvoluted OH* images for Sw = 1.1 at P = 12 kW for different XH_2 with χ = 20%, superimposed with streamlines.

no H_2 is present in the fuel (Case A), the flame stabilizes at a location of y/D = 1 and stretches until y/D = 3. Since it is burning in the inner and the outer shear layer, the flame is classified as a lifted M-flame. As it has been discussed before, the flame is not burning on the centerline, close to the stagnation point. Since a low-velocity region is present, this suggests that the flow features a core with the mixture below the lean flammability limit.

When enriching the fuel with a small amount of H_2, the flame trailing edge in the outer shear layer moves closer to the combustor dump plane, while the tip in the inner shear layer moves further away. When the H_2 content is increased even more up to 80%, both the inner tip and the outer tip of the flame move closer to the combustor dump, while still featuring the shape of an M-flame. For 100% H_2 (Case F), the flame is a Π-flame attached to the outer rim of the injector. Flame F is similar to the low swirl flame observed in the work of Cheng et al. [49], which together with the flow field shown in Fig. 5 suggests that the swirl number is significantly decreased compared to the low H_2 cases.

3.3. NO emission analysis

Fig. 9 shows the NO emissions under various operating conditions for the two different swirl numbers. The average NO values, including the standard deviation, are plotted against the adiabatic flame temperature of the perfectly premixed case. The measurements are presented for increasing power levels, keeping the air flow rate constant, which increases the equivalence ratio ϕ. This results in increased NO emissions due to increased NO formation via the thermal pathway. As flame shapes are strongly influenced by the levels of AAI and XH_2, no relation between the flame shape and emissions can be established.

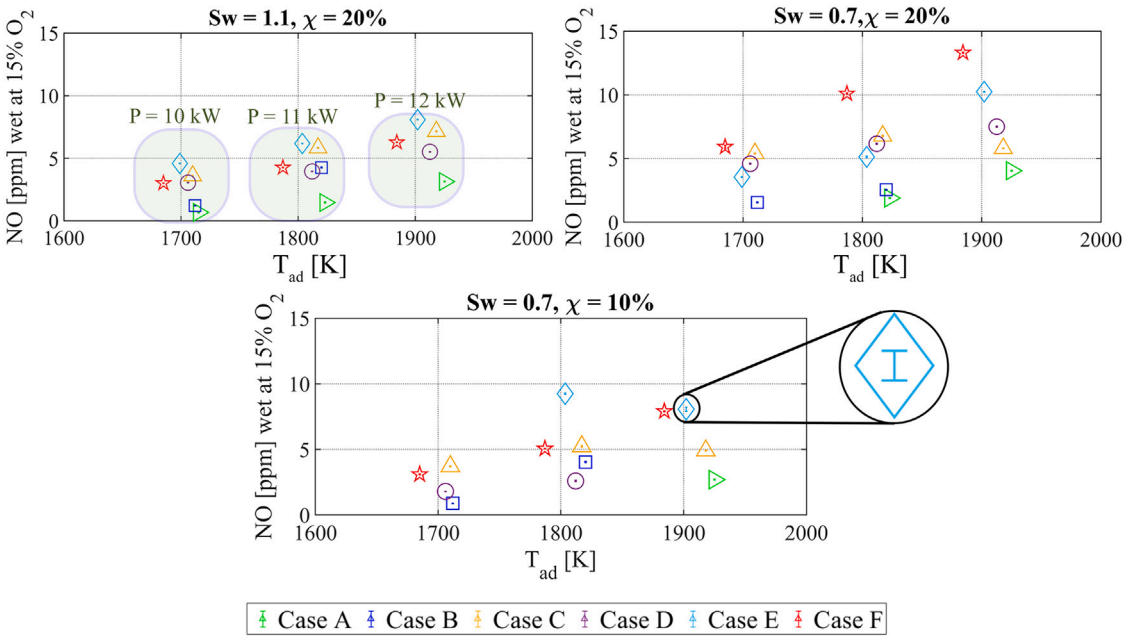

Fig. 9. Average NO emissions and standard deviations for Sw = 0.7 and Sw = 1.1 at different levels of AAI, P and XH_2.

Increasing H_2 content generally leads to increased NO emissions, contradictory to what is expected from calculated adiabatic flame temperatures for the premixed case. The mixing process in jet-in cross-flow configuration is complex, influenced by factors such as the density ratio of fuel–air and the momentum flux ratio J. Increasing H_2 content results in an increasing density ratio of the fuel to the swirling flow and a slight increase in J (see Table 1). This is expected to enhance mixing with the swirling flow [35], which would result in a further decrease in NO emissions for increasing H_2-content.

The trend of increasing NO emissions for increasing H_2 content is particularly evident in the Sw = 0.7, χ = 20% case. Two plausible explanations which combined can explain this trend are proposed. Due to the partially premixed operational mode, flames attached to the injector (Case F) have less time available for mixing. As a result, the local fuel–air mixture is expected to be richer than the nominal equivalence ratio ϕ shown in Table 1. This leads to locally high flame temperatures, and consequently an increased formation of thermal NO. In contrast, flames lifted further from the injector (Case A) benefit from an additional length of y/D = 1 downstream of the mixing tube exit, where mixing can take place. This allows for a more uniform flame temperature and a fuel–air mixture closer to the nominal ϕ, thereby limiting the formation of thermal NO. This means that due to the substantial increase in flame speed, the change in flame position appears to have a greater influence on the NO emissions than the improvement in mixing quality for increasing XH_2. Additionally, as observed in other studies [26,27], a weakened IRZ for increasing H_2 contents can increase the actual flame temperature. This happens due to less or no recirculation of colder products into the reaction zone. Consequently more thermal NO can form. This can outweigh the effect of a lower residence time in the reaction zone for increasing H_2 contents [26].

Overall, for the same level of AAI, the higher swirl number results in lower NO values compared to the lower swirl number (Fig. 9 top row), a trend observed in other studies as well [50]. Higher swirl numbers facilitate better mixing, thereby reducing the locally rich zones. When comparing the plot with Sw = 1.1, χ = 20% with the one of Sw = 0.7, χ = 10%, it can be observed that for the high H_2 content cases (Case E and Case F), the higher swirl number performs slightly better. Since the location of the flame is similar for all flames for cases E and F (see Figs. 3 and 4) it is assumed that the high swirl number with a higher level of AAI still ensures a better mixing of fuel and air. Further investigation on the velocity field in the mixing tube is ongoing, which will allow to assess the effect of AAI on the effective swirl number for different cases. For lower H_2 content fuels, the change in swirl number does not show any significant difference in NO emissions, supporting the assumption that a considerable degree of mixing still takes place within the combustion chamber. Since low H_2 content flames are lifted off the injector, (see Fig. 4), the equivalence ratio at which the reaction takes place is less affected by the flow field and the level of unmixedness in the mixing tube.

4. Conclusions

This paper explores the fuel flexibility (CH_4/H_2) of a laboratory-scale swirl stabilized combustor. The concept of axial air injection (AAI) is utilized to stabilize flames with high H_2 content. Various optical diagnostic techniques and emission gas analyses were employed to investigate the flow field, flame stabilization, and emission performance. The operational ranges of the combustor were examined for different equivalence ratios (ϕ) and H_2 fractions (XH_2) at two different swirl numbers. AAI significantly increases both the lean blowout limit and the flashback limit. As expected, the low swirl number results in flames that stabilize further downstream in the combustion chamber compared to the high swirl number, thus requiring less AAI to prevent flashback. High levels of AAI (20% for Sw = 1.1) are necessary to stabilize 100% H_2 flames. A small operational window is identified, covering the full range from 100% of CH_4 to 100% of H_2.

The flow field analysis revealed significant changes in the overall flow field structure when changing the fuel from CH_4 to H_2 at χ = 20%. While CH_4 flames exhibit an inner recirculation zone (IRZ), which anchors the flame, the IRZ is completely suppressed for the H_2 flame.

In terms of flame stabilization, introducing a high level of AAI changes the flame from a V-flame to a M/Π-flame, which leads to flame extinction on the centerline. This behavior was observed for all H_2 contents investigated. The low momentum flux ratio between the fuel jet and the air jet forces the fuel to remain near the periphery of the mixing tube. Additionally, the introduction of AAI further impairs mixing, leading to a mixture in the core of swirling flow below flammability limit.

Additionally, switching from CH_4 to H_2 results in greater NO emissions, despite lower theoretical adiabatic flame temperatures for perfectly premixed configurations. This is to be expected due to the

CH_4 flame anchoring further downstream in the combustion chamber, allowing more time for fuel and air to mix. Consequently, combustion for high H_2 flames takes place at higher equivalence ratios. The main findings of this study summarized are:

- AAI allows stabilizing flames throughout the full range of 100% CH_4 to 100% H_2.
- Despite allowing for fuel-flexibility, the current configuration does not achieve good mixing. This results in higher NO emissions when compared to a perfectly premixed system, but also in a high risk of boundary layer flashback, since fuel is located close to the periphery of the mixing tube.
- Changing the fuel from 100% CH_4 to 100% H_2 significantly alters the flow field structure. For 100% H_2, the inner recirculation zone is not established in the current configuration.

It is concluded, that AAI can be a suitable approach for fuel-flexible combustion chambers. However, future investigations need to focus on the fuel injection method, to guarantee a better mixing of fuel and air and to stabilize the flame away from the boundary layer of the mixing tube.

CRediT authorship contribution statement

Sarah Link: Writing – review & editing, Writing – original draft, Visualization, Methodology, Investigation, Conceptualization. **Kaushal Dave:** Writing – review & editing, Investigation, Conceptualization. **Francesca de Domenico:** Writing – review & editing, Supervision, Methodology. **Arvind Gangoli Rao:** Writing – review & editing, Funding acquisition, Conceptualization. **Georg Eitelberg:** Writing – review & editing, Supervision.

Declaration of competing interest

The authors declare the following financial interests/personal relationships which may be considered as potential competing interests: All authors report financial support was provided by Safran Tech.

Acknowledgments

This project has been financed by the Dutch Ministry of Economic Affairs and Climate under the TKIscheme (Grant number TKI HTSM/18.0170) along with SAFRAN TECH. The authors would like to acknowledge Nicholas Treleaven and Askin Isikveren from SAFRAN TECH for their contributions to the discussions within the APPU project.

References

[1] Hoelzen J, Silberhorn D, Zill T, Bensmann B, Hanke-Rauschenbach R. Hydrogen-powered aviation and its reliance on green hydrogen infrastructure – review and research gaps. Int J Hydrog Energy 2022;47(5):3108–30. http://dx.doi.org/10.1016/j.ijhydene.2021.10.239, Hydrogen Energy and Fuel Cells.

[2] York WD, Ziminsky WS, Yilmaz E. Development and testing of a low NOx hydrogen combustion system for heavy-duty gas turbines. J Eng Gas Turbines Power 2013;135(2):022001. http://dx.doi.org/10.1115/1.4007733.

[3] Ma N, Zhao W, Wang W, Li X, Zhou H. Large scale of green hydrogen storage: Opportunities and challenges. Int J Hydrog Energy 2024;50:379–96. http://dx.doi.org/10.1016/j.ijhydene.2023.09.021.

[4] Tao M, Azzolini JA, Stechel EB, Ayers KE, Valdez TI. Review—Engineering challenges in green hydrogen production systems. J Electrochem Soc 2022;169(5):054503. http://dx.doi.org/10.1149/1945-7111/ac6983.

[5] Taamallah S, Vogiatzaki K, Alzahrani FM, Mokheimer E, Habib MA, Ghoniem AF. Fuel flexibility, stability and emissions in premixed hydrogen-rich gas turbine combustion: Technology, fundamentals, and numerical simulations. Appl Energy 2015;154:1020–47. http://dx.doi.org/10.1016/j.apenergy.2015.04.044.

[6] Tuncer O, Acharya S, Uhm J. Dynamics, NOx and flashback characteristics of confined premixed hydrogen-enriched methane flames. Int J Hydrog Energy 2009;34(1):496–506. http://dx.doi.org/10.1016/j.ijhydene.2008.09.075.

[7] Rashwan S, Nemitallah M, Habib MA. Review on premixed combustion technology: Stability, emission control, applications, and numerical case study. Energy Fuels 2016;30. http://dx.doi.org/10.1021/acs.energyfuels.6b02386.

[8] Funke HH-W, Beckmann N, Keinz J, Horikawa A. 30 years of dry-low-NOx micromix combustor research for hydrogen-rich fuels"an overview of past and present activities. J Eng Gas Turbines Power 2021;143(7):071002. http://dx.doi.org/10.1115/1.4049764.

[9] Syred N, Beér J. Combustion in swirling flows: A review. Combust Flame 1974;23(2):143–201. http://dx.doi.org/10.1016/0010-2180(74)90057-1.

[10] O Lucca-Negro T. Vortex breakdown: a review. Progress in Energy and Combustion Science 2001;27:431–81. http://dx.doi.org/10.1016/S0360-1285(00)00022-8.

[11] Sayad P, Schönborn A, Klingmann J. Experimental investigation of the stability limits of premixed syngas-air flames at two moderate swirl numbers. Combust Flame 2016;164:270–82. http://dx.doi.org/10.1016/j.combustflame.2015.11.026.

[12] Burmberger S, Sattelmayer T. Optimization of the aerodynamic flame stabilization for fuel flexible gas turbine premix burners. J Eng Gas Turbines Power 2011;133(10). http://dx.doi.org/10.1115/1.4003164.

[13] Reichel TG, Terhaar S, Paschereit O. Increasing flashback resistance in lean premixed swirl-stabilized hydrogen combustion by axial air injection. J Eng Gas Turbines Power 2015;137(7). http://dx.doi.org/10.1115/1.4029119.

[14] Reichel T, Terhaar S, Paschereit C. Flashback resistance and fuel–air mixing in lean premixed hydrogen combustion. J Propuls Power 2018;34:670–701. http://dx.doi.org/10.2514/1.B36646.

[15] Lantz A, Collin R, Aldén M, Lindholm A, Larfeldt J, Lörstad D. Investigation of Hydrogen Enriched Natural Gas Flames in a SGT-700/800 Burner Using OH PLIF and Chemiluminescence Imaging. J Eng Gas Turbines Power 2014;137(3):031505. http://dx.doi.org/10.1115/1.4028462.

[16] Marragou S, Magnes H, Poinsot T, Selle L, Schuller T. Stabilization regimes and pollutant emissions from a dual fuel CH4/H2 and dual swirl low NOx burner. Int J Hydrog Energy 2022;47(44):19275–88. http://dx.doi.org/10.1016/j.ijhydene.2022.04.033.

[17] Marragou S, Magnes H, Aniello A, Selle L, Poinsot T, Schuller T. Experimental analysis and theoretical lift-off criterion for H2/air flames stabilized on a dual swirl injector. Proc Combust Inst 2023;39(4):4345–54. http://dx.doi.org/10.1016/j.proci.2022.07.255.

[18] Schefer RW, Wicksall DM, Agrawal AK. Combustion of hydrogen-enriched methane in a lean premixed swirl-stabilized burner. Proc Combust Inst 2002;29(1):843–51. http://dx.doi.org/10.1016/S1540-7489(02)80108-0.

[19] Abdelwahid S, Nemitallah M, Imteyaz B, Abdelhafez A, Habib MA. On the effects of H2-enrichment and inlet velocity on stability limits and shape of CH4/H2-o2/CO2 flames in a premixed swirl combustor. Energy Fuels 2018;32. http://dx.doi.org/10.1021/acs.energyfuels.8b01958.

[20] Liu C, Cao Z, Li F, Lin Y, Xu L. Flame monitoring of a model swirl injector using 1D tunable diode laser absorption spectroscopy tomography. Meas Sci Technol 2017;28(5):054002. http://dx.doi.org/10.1088/1361-6501/aa5aee.

[21] Imteyaz BA, Nemitallah MA, Abdelhafez AA, Habib MA. Combustion behavior and stability map of hydrogen-enriched oxy-methane premixed flames in a model gas turbine combustor. Int J Hydrog Energy 2018;43(34):16652–66. http://dx.doi.org/10.1016/j.ijhydene.2018.07.087.

[22] Liu X, Bertsch M, Subash AA, Yu S, Szasz R-Z, Li Z, et al. Investigation of turbulent premixed methane/air and hydrogen-enriched methane/air flames in a laboratory-scale gas turbine model combustor. Int J Hydrog Energy 2021;46(24):13377–88. http://dx.doi.org/10.1016/j.ijhydene.2021.01.087.

[23] An Q, Kheirkhah S, Bergthorson J, Yun S, Hwang J, Lee WJ, et al. Flame stabilization mechanisms and shape transitions in a 3D printed, hydrogen enriched, methane/air low-swirl burner. Int J Hydrog Energy 2021;46(27):14764–79. http://dx.doi.org/10.1016/j.ijhydene.2021.01.112.

[24] Mao R, Wang J, Zhang W, An Z, Lin W, Zhang M, et al. Effect of high hydrogen enrichment on the outer-shear-layer flame of confined lean premixed CH4/H2/air swirl flames. Int J Hydrog Energy 2021;46(34):17969–81. http://dx.doi.org/10.1016/j.ijhydene.2021.02.181, Special issue on the 2nd International Symposium on Hydrogen Energy and Energy Technologies (HEET 2019).

[25] Guo S, Wang J, Zhang W, Zhang M, Huang Z. Effect of hydrogen enrichment on swirl/bluff-body lean premixed flame stabilization. Int J Hydrog Energy 2020;45(18):10906–19. http://dx.doi.org/10.1016/j.ijhydene.2020.02.020.

[26] Kim H, Arghode V, Linck M, Gupta A. Hydrogen addition effects in a confined swirl-stabilized methane-air flame. Int J Hydrog Energy 2009;34(2):1054–62. http://dx.doi.org/10.1016/j.ijhydene.2008.10.034.

[27] Kim H, Arghode V, Gupta A. Flame characteristics of hydrogen-enriched methane–air premixed swirling flames. Int J Hydrog Energy 2009;34(2):1063–73. http://dx.doi.org/10.1016/j.ijhydene.2008.10.035.

[28] Park S. Hydrogen addition effect on NO formation in methane/air lean-premixed flames at elevated pressure. Int J Hydrog Energy 2021;46(50):25712–25. http://dx.doi.org/10.1016/j.ijhydene.2021.05.101.

[29] Wang D, Tan Z, Xu J, Meng H. Quantitative studies of NO emissions from various reaction pathways in swirling combustion of hydrogen-enriched methane. Int J Hydrog Energy 2024;53:409–21. http://dx.doi.org/10.1016/j.ijhydene.2023.12.001.

[30] Mao R, Wang J, Lin W, Han W, Zhang W, Huang Z. Effects of flow–flame interactions on the stabilization of ultra-lean swirling CH4/H2/air flames. Fuel 2022;319:123619. http://dx.doi.org/10.1016/j.fuel.2022.123619.

[31] Broadwell J, Breidenthal R. Structure and mixing of a transverse jet in incompressible flow. J Fluid Mech 1984;148:405–12. http://dx.doi.org/10.1017/S0022112084002408.
[32] Ferrante G, Doodeman L, Rao AG, Langella I. LES of Hydrogen-Enriched Methane Flames in a Lean-Burn Combustor With Axial Air Injection. In: Turbo expo: power for land, sea, and air. Combustion, fuels, and emissions, vol. 3B, 2023, http://dx.doi.org/10.1115/GT2023-103006.
[33] Link S, Dave K, Eitelberg G, Gangoli Rao A, de Domenico F. The Influence of the Confinement Ratio on the Precessing Vortex Core Dynamics in a Counter-Rotating Dual Swirler. In: Turbo expo: power for land, sea, and air. Combustion, fuels, and emissions, vol. 3B, 2023, http://dx.doi.org/10.1115/GT2023-101678.
[34] Beér J, Chigier N. Combustion Aerodynamics [by] J.M. Beér and N.A. Chigier. In: Fuel and energy science series, Applied Science Publishers Limited; 1972.
[35] So RMC, Ahmed SA. Helium jets discharging normally into a swirling air flow. Exp Fluids 1987;5:255–62. http://dx.doi.org/10.1007/BF00279739.
[36] Goodwin DG, Moffat HK, Schoegl I, Speth RL, Weber BW. Cantera: An object-oriented software toolkit for chemical kinetics, thermodynamics, and transport processes. 2023, http://dx.doi.org/10.5281/zenodo.8137090, Version 3.0.0 https://www.cantera.org.
[37] Simons S, Yuan Z-G. The filtered abel transform and its application in combustion diagnostics. Tech. rep., Cleveland, United States: NASA Glenn Research Center Cleveland; 2003.
[38] Sardeshmukh S, Bedard M, Anderson W. The use of OH* and CH* as heat release markers in combustion dynamics. Int J Spray Combust Dyn 2017;9(4):409–23. http://dx.doi.org/10.1177/1756827717718483.
[39] Baulch D, Cobos C, Cox R, Frank P, Hayman G, Just T, et al. Evaluated kinetic data for combustion modeling. Supplement i. J Phys Chem Ref Data 1994;23:847–8. http://dx.doi.org/10.1063/1.555953.
[40] Benim A, Syed K. Flashback mechanisms in lean premixed gas turbine combustion. Elsevier Science; 2014, URL https://books.google.nl/books?id=o3ODBAAAQBAJ.
[41] Schefer R, Kulatilaka W, Patterson B, Settersten T. Visible emission of hydrogen flames. Combust Flame 2009;156(6):1234–41. http://dx.doi.org/10.1016/j.combustflame.2009.01.011.
[42] Fiala T, Sattelmayer T. Heat release and UV–Vis radiation in non-premixed hydrogen–oxygen flames. Exp Fluids 2015;56:144. http://dx.doi.org/10.1007/s00348-015-2013-8.
[43] Billant P, Chomaz J-M, Huerre P. Experimental study of vortex breakdown in swirling jets. J Fluid Mech 1998;376:183–219. http://dx.doi.org/10.1017/S0022112098002870.
[44] Syred N, Chigier NA, Beér JM. Flame stabilization in recirculation zones of jets with swirl. Symp (Int) Combust 1971;13(1):617–24. http://dx.doi.org/10.1016/S0082-0784(71)80063-2.
[45] Shoji T, Iwasaki Y, Kodai K, Yoshida S, Tachibana S, Yokomori T. Effects of flame behaviors on combustion noise from lean-premixed hydrogen low-swirl flames. AIAA J 2020;58:1–17. http://dx.doi.org/10.2514/1.J059049.
[46] Guiberti TF, Durox D, Zimmer L, Schuller T. Analysis of topology transitions of swirl flames interacting with the combustor side wall. Combust Flame 2015;162(11):4342–57. http://dx.doi.org/10.1016/j.combustflame.2015.07.001.
[47] Mercier R, Guiberti T, Chatelier A, Durox D, Gicquel O, Darabiha N, et al. Experimental and numerical investigation of the influence of thermal boundary conditions on premixed swirling flame stabilization. Combust Flame 2016;171:42–58. http://dx.doi.org/10.1016/j.combustflame.2016.05.006.
[48] Terhaar S, Reichel TG, Schrodinger C, Rukes L, Oberleithner K, Paschereit CO. Vortex breakdown and global modes in swirling combustor flows with axial air injection. In: 43rd fluid dynamics conference. Reston, Virginia: American Institute of Aeronautics and Astronautics; 2013, p. 219–29. http://dx.doi.org/10.2514/6.2013-2602.
[49] Cheng R, Littlejohn D, Strakey P, Sidwell T. Laboratory investigations of a low-swirl injector with H2 and CH4 at gas turbine conditions. Proc Combust Inst 2009;32(2):3001–9. http://dx.doi.org/10.1016/j.proci.2008.06.141.
[50] Schmittel P, Günther B, Lenze B, Leuckel W, Bockhorn H. Turbulent swirling flames: Experimental investigation of the flow field and formation of nitrogen oxide. Proc Combust Inst 2000;28(1):303–9. http://dx.doi.org/10.1016/S0082-0784(00)80224-6.